(E.14) is discretised according to a central difference technique (Appendix H).

The dissipation or irreversible work is related partly to the friction factor which accounts for the shear work terms. The normal stress terms are again included to modify the steady, incompressible and isothermal empirical term.

From Appendix E the expression for E is as follows:

$$E = V\mu\{2(g\ v)^2 Fr/d^2 + \frac{4}{3}\left[\frac{\partial}{\partial x}(g\ v)\right]^2\} \qquad (E.31)$$

Note that E is always positive.

(E.31) is discretised in Appendix H according to central difference techniques.

Another form of dissipation not frequently appreciated is that due to eddies. This is often catered for in steady flow work by simply defining irrecoverable pressure loss coefficients [KL64]. It must be noted here that a simple pressure loss coefficient cannot be defined for non-steady flow systems. The reason for this is that the pressure drop so defined represents the integrated pressure loss over an infinite time. In non-steady flow systems it is better to relate the 'irrecoverable pressure loss' to the dissipation in the energy equation. After all this is in fact what it is.

A technique is suggested in Appendix E to relate empirical coefficients for contraction and expansion losses to the dissipation work. The result is as follows:

$$E = |g^3|A\ v^2 K/2 \qquad (E.25)$$

where K is the standard contraction or expansion coefficient given by Kays and London [KL64].

Equation (E.25) is applied at any point in the flow where an abrupt change in flow area occurs.

Urieli *et al* [Ur77, UR77] and Schock [Sc77] both define an irrecoverable pressure drop.

The convective heat transfer is calculated from the Reynolds' Analogy which was also used by Urieli [Ur77]. Other analogies may be used, but for Prantdl numbers around 0,7 the improvement would be marginal.

The definition of the heat transfer coefficient is:

$$dq/dz = h\ Awg(Tw - T) \qquad (3.12)$$

From the Reynolds' analogy (Appendix E) the heat transfer coefficient is given by:

$$h = k\ Fr/(2d) \qquad (E.35)$$

Heat transfer coefficients for the working spaces are discussed in Appendix E. However, they were found to be unsatisfactory and all simulation runs were made under the assumption of adiabatic working spaces.

3.7 System Algorithms

All the discretised equations which define the system are given in Appendix H. Following the procedure suggested by Urieli [Ur77], the equivalent FORTRAN statements are included for each discretised equation. The FORTRAN statements are not general in that they have been derived specifically for

simulating the experimental rig used in this work.

The variation of the transport properties with temperature are given in Appendix F.

All the parameters used in the computer simulation programme have been normalised according to the system suggested by Urieli [Ur77, UR77]. This system has been found to give extremely small round-off error [Go77]. A full discussion and description of the normalising system plus the equivalent computer parameters can be found in Appendix G.

3.8 The Method of Solution

Since the equations required to be solved form a set of simultaneous first order differential equations, it is possible to use explicit numerical methods.

Urieli [Ur77, UR77] has used the classical Runge Kutta technique. This has been shown to work well, albeit a bit slow, and it has been used exclusively in this work (Appendix I).

Modern lower order Runge Kutta techniques such as those suggested by Fehlberg [Fe69] may prove to be much faster with an acceptable increase in truncation error. Urieli [Ur77, UR77] suggested a method of forcing the system to converge within a small number of cycles. This is based on the requirement that at cyclically steady state there is no net cyclic heat transferred between the gas and the regenerator. After each cycle the residual heat transferred to the regenerator is used to alter the regenerator cell temperatures in such a way so as to reduce this residual heat transfer to zero. The

procedure is fully described in Appendix I.

3.3 Summary and Conclusions

The mechanical arrangement chosen for simulation in this work is the alpha configuration.

Different simulation techniques were discussed, and it was argued that the integral approach is more flexible, economical and mathematically more tractable.

Urieli's equations were discussed, it was shown that certain intuitive reasoning was required to discretise these equations. The integral equations derived in this work were shown to reduce to the same discretised equations used by Urieli for continuity and energy without intuitive reasoning.

The final form of the momentum equation used by Urieli did however not agree with the integral momentum equations derived in this work.

The empirical factors have been modified by the inclusion of the normal stress terms. Both the viscous friction and the dissipation have been modelled in this manner. Eddy dissipation is included in the energy equation and this is shown to account for the so-called irrecoverable pressure drop found in steady flow systems.

The system algorithms (presented in Appendix H) were derived specifically for the experimental rig.

The classical fourth-order Runge Kutta explicit integration scheme is used to integrate the system of equations. To reach cyclically steady state, the convergence system developed by Urieli is used.

4 THE EXPERIMENTAL SIMULATION RIG

4.1 Introduction

The simulation technique developed in this work is completely general in that it can simulate any machine in which a body of gas is subjected to a similar cycle to that found in Stirling machines. This offers great flexibility in that it is not necessary to design a sophisticated working example of a Stirling engine (or refrigerator, or heat pump) to experimentally validate the analysis. It is more convenient to design a Stirling cycle simulation rig around the available transducers and measuring equipment, taking into account the operating temperature range and time constants of the various instruments.

In this work, such a rig has been used exclusively for verification of the analytical procedures presented.

4.2 Description of the Experimental Rig

The experimental rig is based on the alpha arrangement pseudo-Stirling cycle. Two piston-cylinder assemblies are communicated to each other by way of seven continuous copper tubes. These tubes serve alternately as the cooler, regenerator and heater. No effort is made to cool or heat the gas in the working spaces. A crank shaft and connecting rod assemblies drive the pistons, and the relative angle of the piston motions may be varied in 45^{o} steps.

The gas temperatures in Stirling machines vary over a large range which has a consequent effect on the transport properties (see Appendix F). Thus it is important that the rig also operates with a temperature range large enough such that the effect on the transport properties becomes noticeable. This is achieved

by condensing steam on the heater section and sublimating 'dry ice' (solid carbon dioxide) on the cooler section. The dry ice is placed in an acetone bath so as to obtain a reasonable isothermal wall condition.

The regenerator section is thermally insulated from the environment. Regeneration takes place directly to the walls of the copper tubes and no matrix is included.

The machine is incapable of producing enough power to drive itself, thus a small half kilowatt dc electric motor is used to supply the necessary driving power. A heavy flywheel is incorporated to avoid speed fluctuations which was designed to provide less than 5% speed variation at 2 Hz. The maximum operating frequency is 4,5 Hz at which point flow-induced compressibility effects start becoming noticeable.

The basic rig was designed by Bawa and Joshi [BJ76] and their calculations are not repeated in this work. The original design only included one copper tube communicating the working spaces to each other and no attempt was made to include facilities for the determination of an energy balance. Modifications were thus necessary and these were as follows:-

1) Seven copper tubes were installed between the working cylinders, as has been previously noted. This was done to increase the heat transfer and flow friction to effective levels.

2) Dummy piston heads were installed to reduce heat losses through the pistons and to shield the working gas from the heat generated by seal friction.

3) To further reduce the effects of seal frictional heating, cylinder cooling jackets were installed.

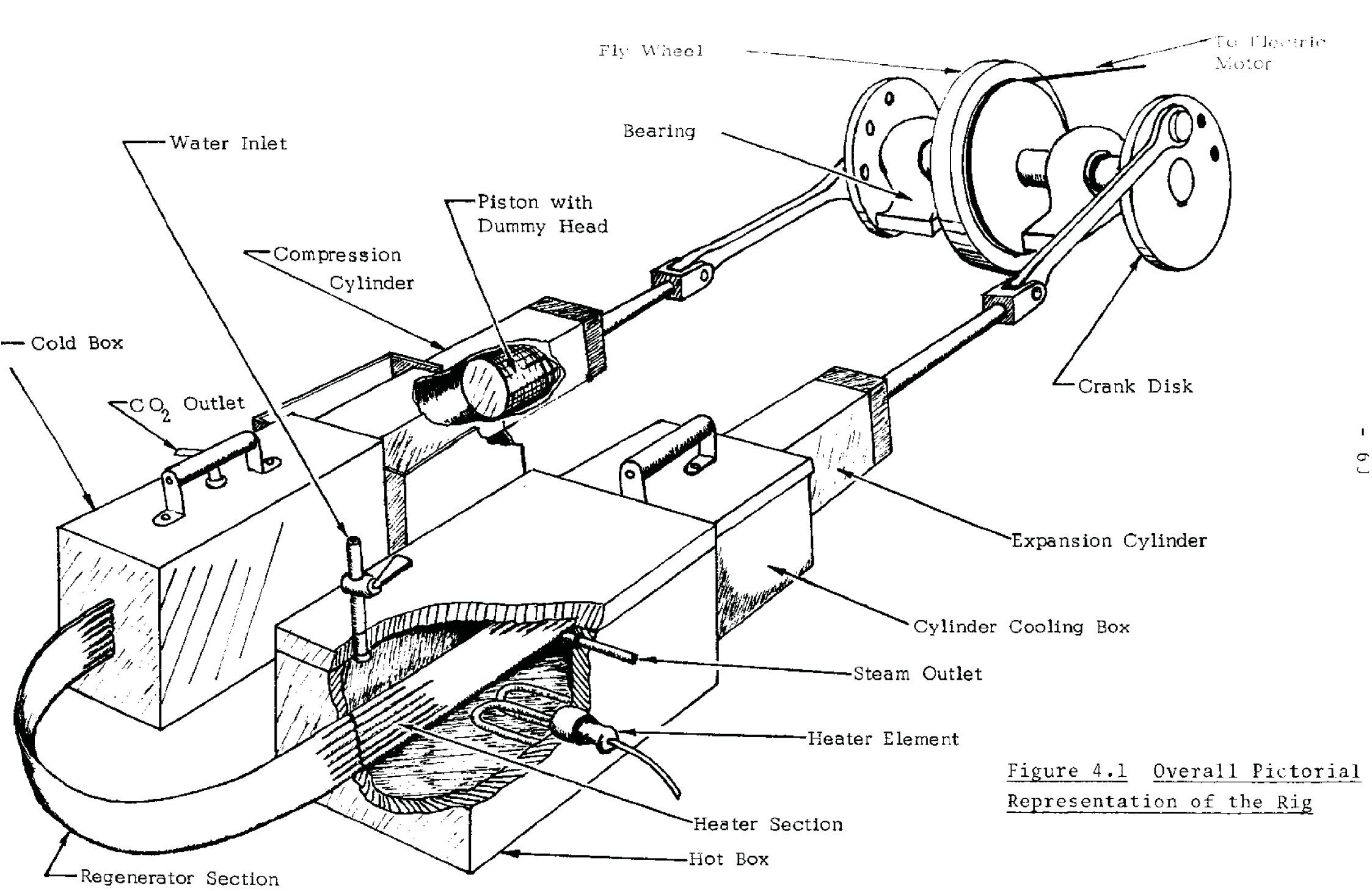

Figure 4.1 Overall Pictorial Representation of the Rig

4) The thermal insulation was extended to include the cooler and heater boxes.

5) Both cooler and heater were entirely enclosed except for the carbon dioxide gas outlet on the cooler box and the water inlet and steam outlet on the heater box.

6) A condenser was installed for condensing the steam.

7) Provision was made for varying the speed of the dc driving motor.

Dimensional assembly and various detailed drawings are included in Appendix K. An overall pictorial representation of the rig is shown in Figure 4.1.

4.3 Geometric Specifications of the Experimental Rig

The working spaces are identical, thus for each working space:

Stroke = 0,192 m
Connecting rod length = 0,384 m
Piston face area = $0{,}25670.10^{-2} m^2$

From this the total stroke volume (ie, the sum of the stroke volumes for each working space) $Vs = 9{,}8573.10^{-4} m^3$.

The following specifications are common to all the heat exchangers:

number of tubes = 7
average inside diameter = $0{,}4800.10^{-2}$ m
average outside diameter = $0{,}64666.10^{-2}$ m
material = copper
density = 8941,00 kg/m^3

specific heat = 393,60 J/kg K
thermal conductivity = 386,30 W/mK
manufacturing technique is cold drawn, hence surface finish has been taken as smooth.

Regenerator:
gas volume = $9{,}972.10^{-5} m^3$

Cooler:
gas volume = $4{,}625.10^{-5} m^3$

Heater:
gas volume = $4{,}625.10^{-5} m^3$

Clearance spaces:

The clearance volume is the volume between the piston at TDC and the associated heat exchanger, in both cases this is: $1{,}971.10^{-5} m^3$.

The fractional dead volume and the fractional clearance volumes are thus:

Vd = 0,235
Vcl = 0,020

4.4 Operating conditions

Expansion space volume phase angle advance:

$\alpha = \pi/2$ rad

Working gas used: Air

Ratio of specific heats γ = 1,4
Gas constant R = 287,0 J/kg K
Average Prandtl number Pr = 0,71
Sutherland constant Tsu = 112 K
Dynamic viscosity at 350 K = 20,66 x 10^{-6} kg/m s

The hot source and cold sink temperatures were maintained by condensing steam and sublimating dry ice respectively. Thus these temperatures were dependent on local variations in the atmospheric pressure. In general they were approximately:

T_{wk} = 199,86 K
T_{wh} = 366,56 K

The values for T_{wk} and T_{wh} were determined for each test run.

4.5 Instrumentation

The areas of greatest uncertainty in the computer simulation are the determination of the friction factors and the heat transfer coefficients. Broadly speaking, the effects of the friction factor are to a large degree indicated by the pressure drop across the system, while the heat transfer coefficients determine the temperature profile along the regenerator. Furthermore, both the friction factor and heat transfer coefficient relate directly to the work done and heats transferred by the system. It was therefore decided to design the experiments as follows (referring to Figure 4.2):

1) The temperature profile along the machine walls would be measured.

2) The instantaneous pressures would be measured at the working spaces.

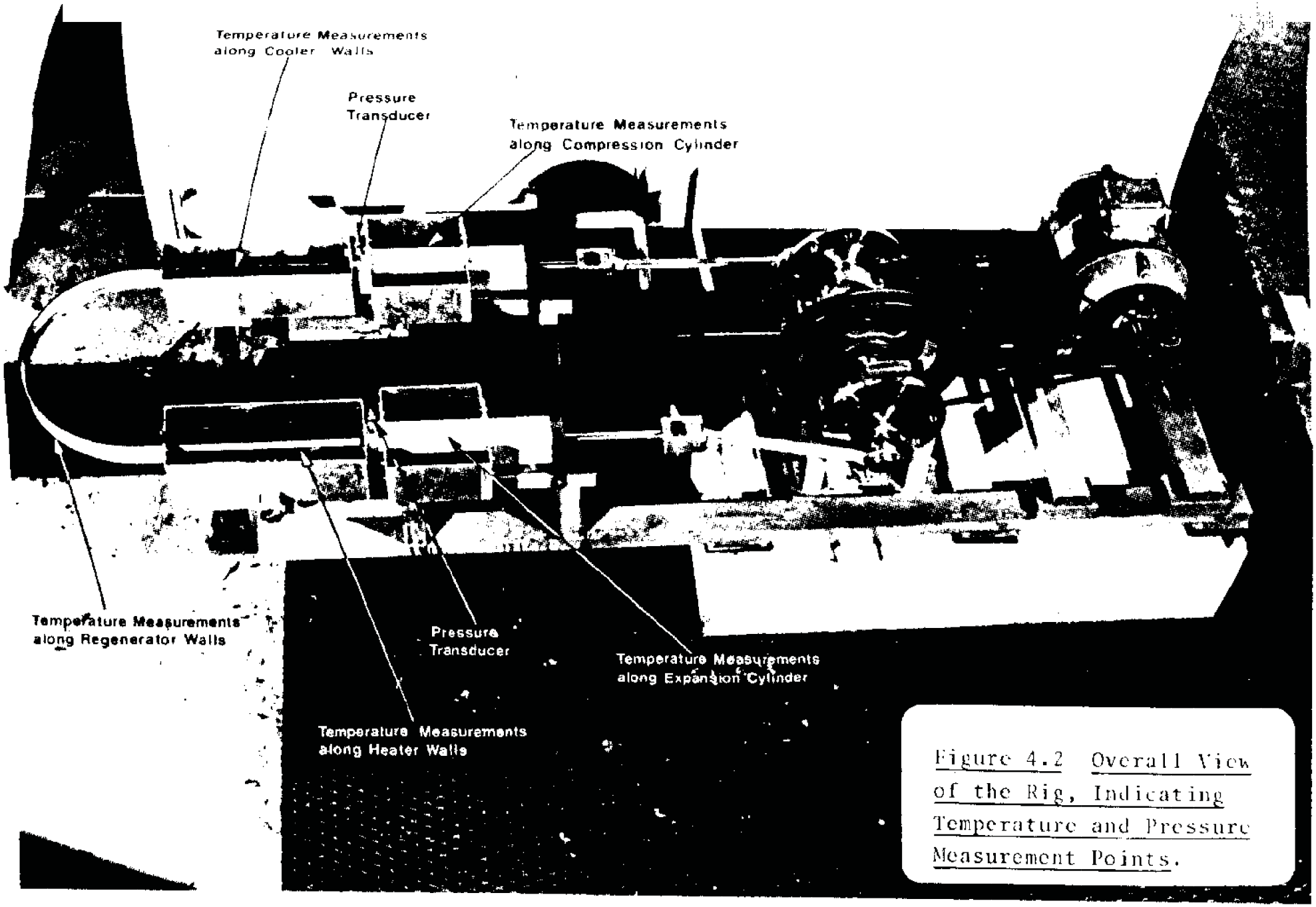

Figure 4.2 Overall View of the Rig, Indicating Temperature and Pressure Measurement Points.

5) The overall energy balance would be determined.

6) The speed of the machine would be measured to investigate the computer simulation's ability to indicate how this affects the heat transfer and the pressure drop.

All the experiments were considered from the point of view of minimum flow interruptions. Gas flow velocities and gas temperatures were considered as additional comparison points. These measurements do, however, interfere with the flow and in any event, they are not fundamental to the validation of the model in the first instance.

Thermocouples were used for all temperature measurements. To obtain the average temperature at each measurement section along the heat exchangers, one thermocouple was connected to each heat exchanger tube at a particular station, the seven thermocouples were then connected to each other in parallel. For increased accuracy it may have been better to connect these thermocouples in series, however an accuracy of within $\pm$ 0,5°C was considered quite reasonable and is easily obtained with the present circuit. Note that the time constants of the thermocouples are not important since the walls of the heat exchangers have sufficient thermal inertia to dampen out these effects. The outputs of the thermocouples were recorded by a Fluke datalogger (specifications given in Appendix L).

A photograph showing the thermocouple installation is given in Figure 4.3 and the circuit diagram is given in Figure 4.4.

Pressures were measured by two Kistler piezo crystal pressure transducers, located at the compression and expansion spaces respectively (Figure 4.2). Kistler charge amplifiers were used to convert the piezo charge to a measurable voltage.

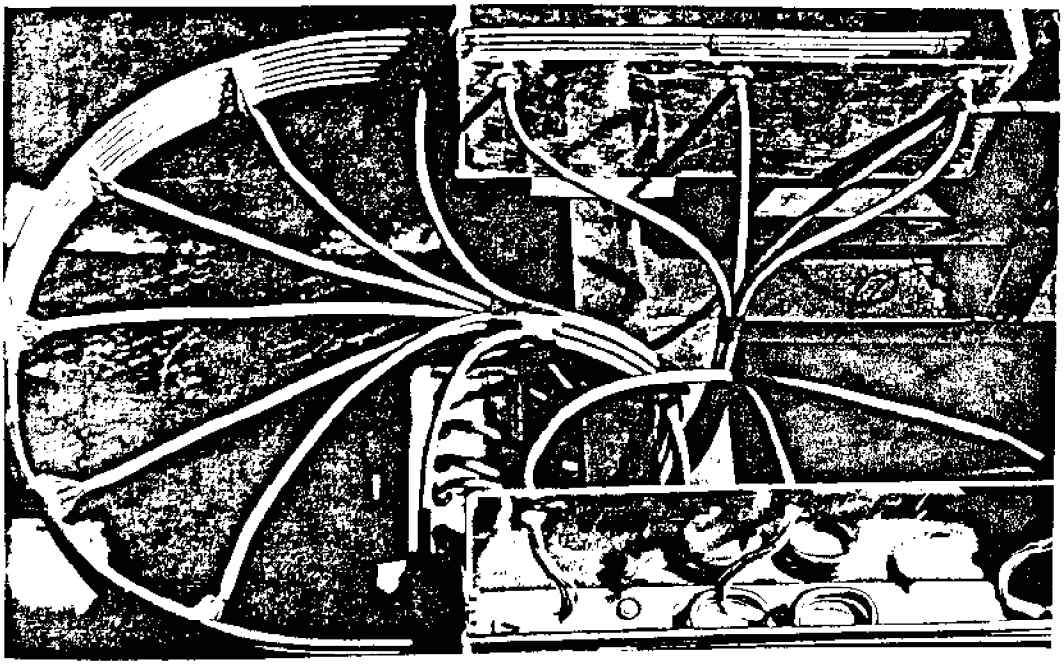

Figure 4.3 Thermocouple Installation

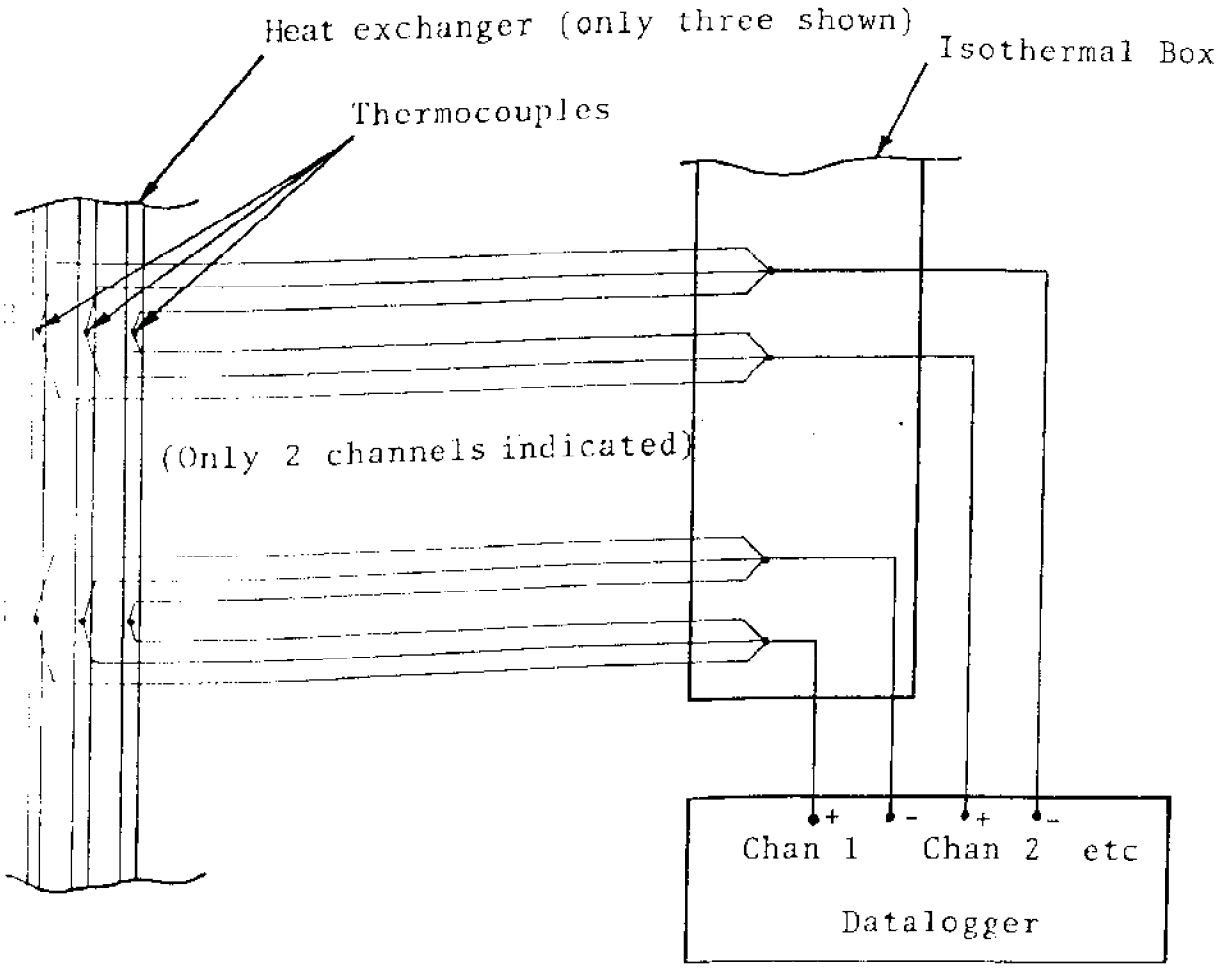

Figure 4.4 Thermocouple Circuit

The output was available on one of two displays: either a two channel Tektronix oscilloscope or, for increased accuracy, a strip chart recorder by way of a Biomation transient recorder. The transient recorder was necessary since the strip chart recorder did not have the required response.

The schematic arrangement for the pressure recording apparatus is shown in Figure 4.5.

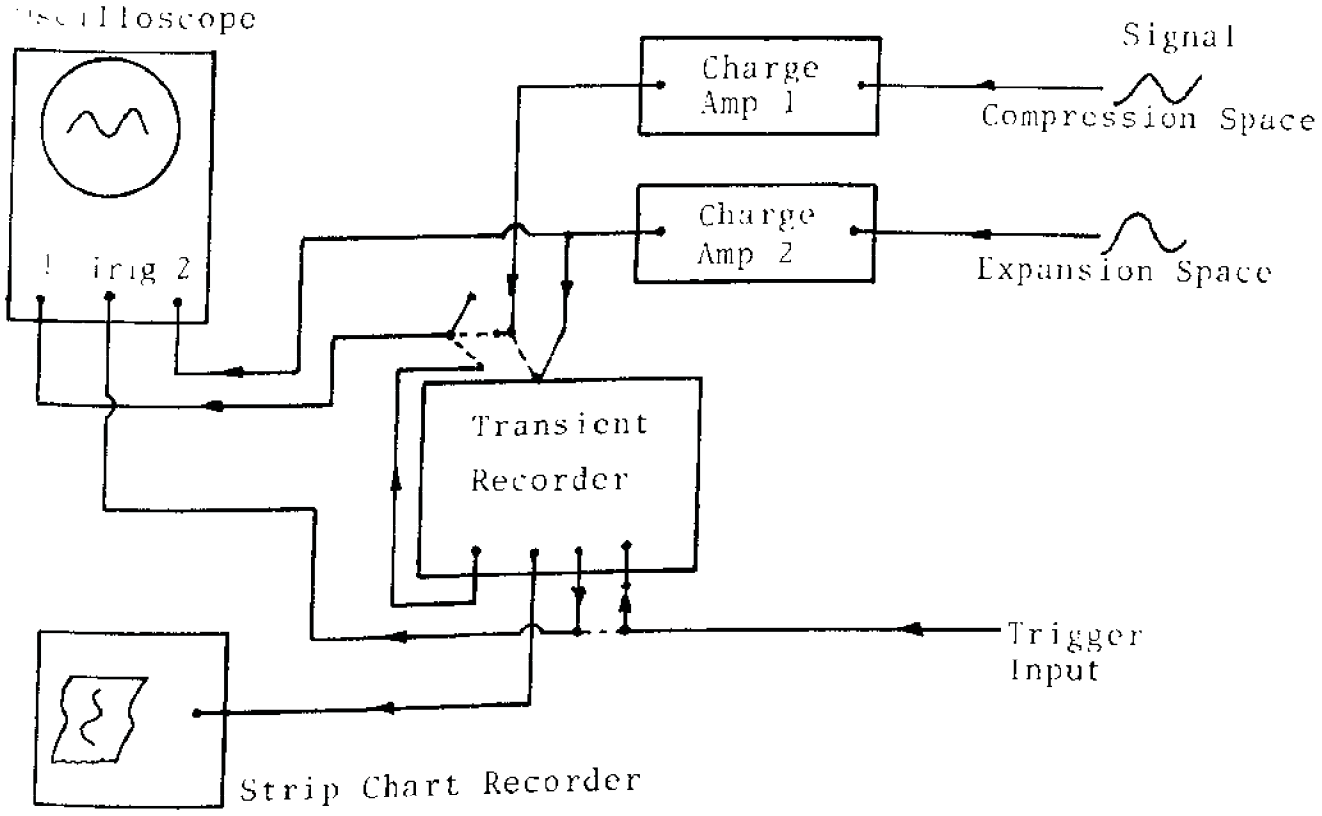

Figure 4.5 Pressure Recording Apparatus

The specifications of all the pressure measuring equipment are given in Appendix L.

The triggering of the instruments for recording the pressure profiles was activated by an opto-electrical switch. A short arm on the crank disk was arranged so that at maximum compression space volume the switch would be activated (Figure 4.6).

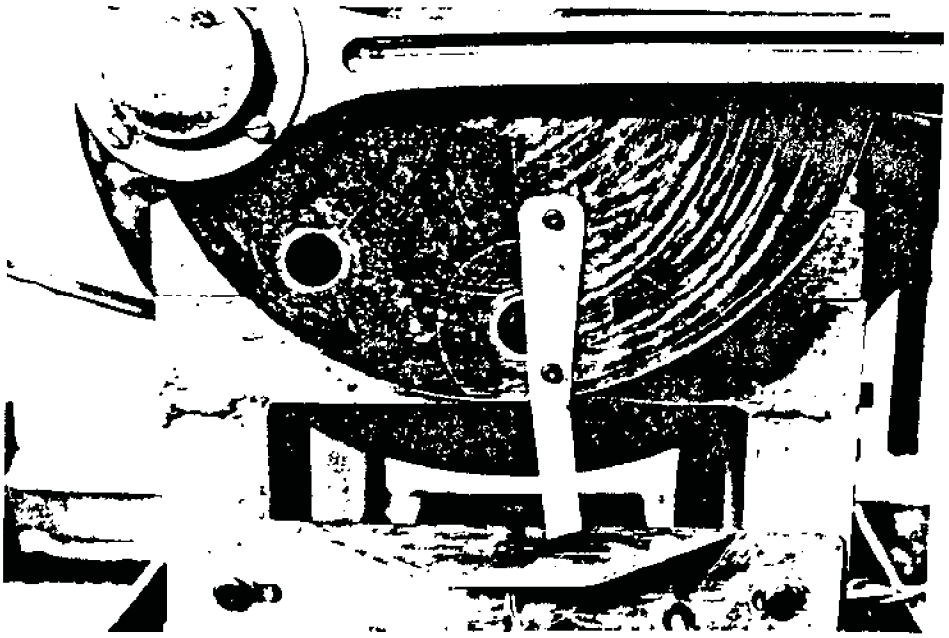

Figure 4.6 Pressure Profiles Triggering Switch

A transistor switch was used to increase the output voltage to 4,5 Volts. The circuit is shown in Figure 4.7.

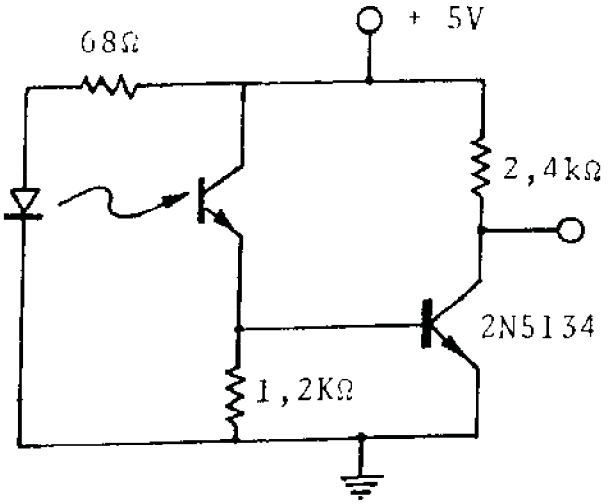

Figure 4.7 Transistor Switch Circuit

The speed of the dc motor was controlled by a variable voltage unit. Provision was made for reversal so that the rig may be run as a heat pump at a future stage. The speed control unit was modified from a circuit designed by Bieniawski [Bi63], the circuit diagram is not included in this work.

The operating speed of the rig was determined by using an opto-electrical switch and a disk fitted onto the crank-shaft which has twenty holes acting as optical interruptions. The output from the opto-electrical switch was taken by way of a transistor switch (as previously described) to a Racal digital frequency meter. The speed of the rig could thus be directly read. The installation arrangement is shown in Figure 4.8.

The specifications of the digital frequency meter are given in Appendix L.

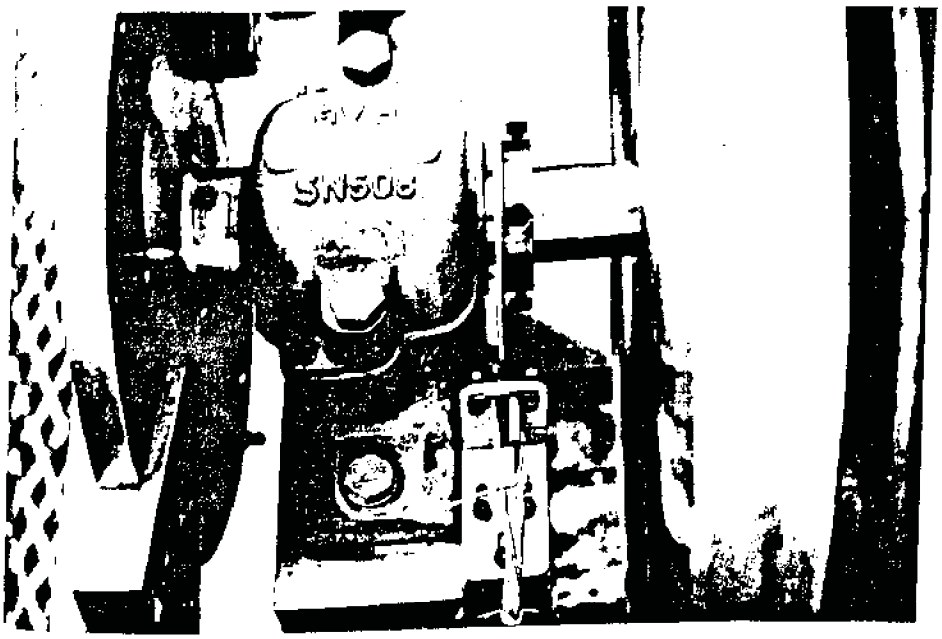

Figure 4.8 Speed Measuring Transducer

The energy quantities measured for the energy balances are: the indicated work, the heat input at the heater and the heat extracted at the cooler.

The indicated work is calculated directly from the measured pressure profiles and the known volume variations.

The heat extracted and the heat input are both calculated by constructing a control volume for each heat exchanger. All energy quantities crossing the boundaries of the control volume must either be calculated or measured.

For the cold end, this requires that the energy being removed by the carbon dioxide gas be determined by measuring its mass flow rate. This was done by the use of an industrial gas meter which measures the volume of gas passed through it. By knowing the pressure and temperature at the gas meter and the duration of a test run it is possible to calculate the mass flow rate. The installation is shown in Figure 4.9.

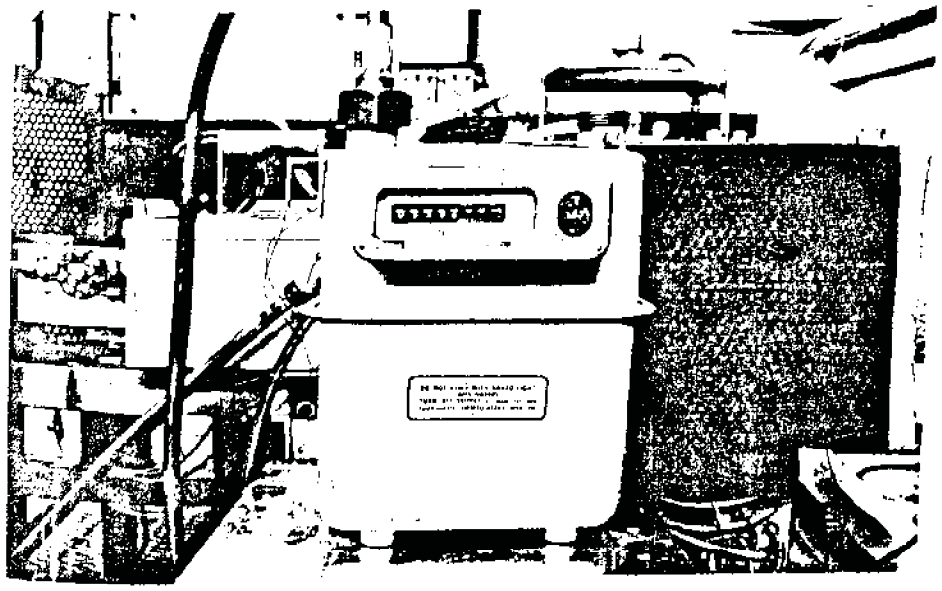

Figure 4.9 The Gas Meter Used for Determining the Volume of Carbon Dioxide Gas

Conduction losses to the regenerator and compression space cylinder are determined by the relevant temperature gradients which are calculated from the temperature profile along the machine.

By taking readings for both running and stationary conditions of the rig, it is possible to determine the heat energy

removed by the cooler. This procedure removes the need to determine the conduction losses through the insulation. The method is fully detailed in Appendix M.

The hot end is treated similarly. The electrical energy input to the heater element is measured by a Weston ac and dc wattmeter. The energy carried out by the steam is determined from the mass of condensate collected over a test run. The condenser is a simple 'shell and tube' type heat exchanger - the arrangement is shown in Figure 4.10.

Conduction losses are accounted for in the same way as for the cooler, and again it is necessary to do running and stationary tests as detailed in Appendix M.

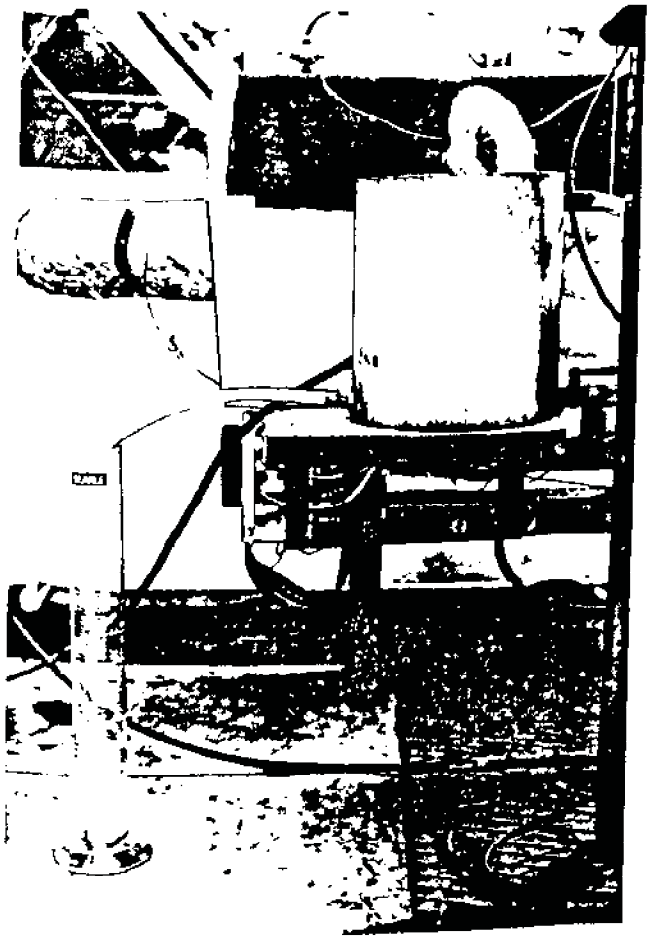

Figure 4.10 Condenser Installation

4.6 Sensitivity and Highest Expected Errors of the Experiments

An error and sensitivity analysis of all the experiments is covered in Appendix O.

The results of this analysis indicate that the highest expected errors for the worst cases are:

Heat extracted from the cold end: $\pm$ 2,4%
Heat added at the hot end: $\pm$ 7,0%

Quantitative figures for the sensitivity were not determined. However, the analysis does indicate an overall sensitivity to the determination of the areas for conduction, especially for the cooler. For the heater, the error in determining the electrical energy input predominates. This error is due to local line voltage fluctuations.

A representative average highest expected error was determined for the following:

Pressure profiles: $\pm$ 1%
Indicated work rate profile: $\pm$ 5,3%
Cyclic indicated work: $\pm$ 5,3%

5 EXPERIMENTAL PROCEDURE

5.1 Introduction

Owing to the lengthy time required for thermal equilibrium, it is necessary to determine some condition at which it can be deemed that thermal equilibrium has been reached. This condition was taken as being an average variation of $\pm$ 0,1°C in two minutes at any point on the heat exchangers. After thermal equilibrium had been reached, all the required observations were made - this took about thirty minutes. The interrelated nature of the experiments required that they be run concurrently or at least during the same test. Thus if any reading or measurement was found to be unsatisfactory after a test run, all the readings taken during that particular run were rejected. It was therefore necessary to develop a strict procedure list to avoid any experimental omissions.

5.2 Preliminary

Set-up procedures were as follows:

1) All instruments and measuring equipment were switched on at least one hour before any test runs were commenced. This was to ensure thermal stability of the equipment.
2) Five litres of water were measured out into the heater box from the supply jar.
3) The cooling water circuit was turned on. The water supply to the condenser and cylinder jackets was adjusted to a steady flow and trickle respectively.
4) The heater element was switched on.
5) Acetone was poured into the cooler box and pieces of dry ice were placed in the acetone until the cooler tubes were covered. Dry-ice was continually added to the acetone until the cold end temperature stabilised. The cooler box was

then carefully sealed with the lid which was secured by eleven wing nuts.

6) Once thermal equilibrium had been reached the stationary tests were commenced.

7) After the completion of the stationary tests, the running tests were executed. Observations were made during three consecutive test runs, each at a different speed (the desired speed was obtained by adjusting the coarse and fine Variacs). Since thermal equilibrium is more rapidly reached at high speeds, the test at the highest speed was done first and the speed was then adjusted to a lower setting for each consecutive test.

5.3 Pressure Profiles

The procedure for recording the pressure profiles was as follows:

1) Both charge amplifiers were set to 'reset' (this destroys any stray charges).

2) The transducer sensitivity settings were checked on the charge amplifiers which were calibrated to give an output of 10 bars per volt.

3) The Biomation transient recorder was set for a range of 100 mV and a sweep of 500 ms. This was found to give the best overall usage of the storage bits.

4) Since the output of the triggering circuit was negative with respect to the Biomation, the trigger was adjusted to a negative slope and a slightly negative level.

5) The 1 V range and a chart speed of 180 mm/min were selected on the Toa strip chart recorder. The chart recorder was only required during playback of the Biomation, thus the precaution was taken to switch the chart drive off when not required.

6) Once thermal equilibrium had been attained, the pressure traces were recorded. This was done by connecting either the expansion or compression space charge amplifier to the Biomation. The single sweep mode was selected, and the charge amplifier was set to 'operate'. The 'arm' button was then pressed. Care was taken to ensure that the signal did not exceed the limits of the selected range. These limits are indicated by two lights on the panel: one for a positive limit and one for a negative limit. The vertical adjustment knob was used to bring the signal between the limits.

7) The oscilloscope provided an easy-to-check image of the trace as recorded by the Biomation. Once it was established that the trace was satisfactory, it was plotted on the strip chart recorder.

8) This procedure was repeated for the second trace.

The length of a test run was found to be too long for the Kistler pressure transducers to sustain the static component of the pressure trace. The static component eventually decays and it was therefore important to relate the cyclic range to the mean (charge) pressure in the system. This was done by selecting a slow sweep rate on the Biomation and then switching the driving motor off - at the same time triggering the pressure trace and opening the air cocks. The pressure in the rig thus decayed to the ambient atmospheric pressure, and the trace thus gave the cyclic pressure decay as the machine came to rest. From this trace it was possible to determine the average cyclic pressure in the rig.

Examples of two pressure traces and a decaying pressure trace are given in Figures 5.1, 5.2 and 5.3.

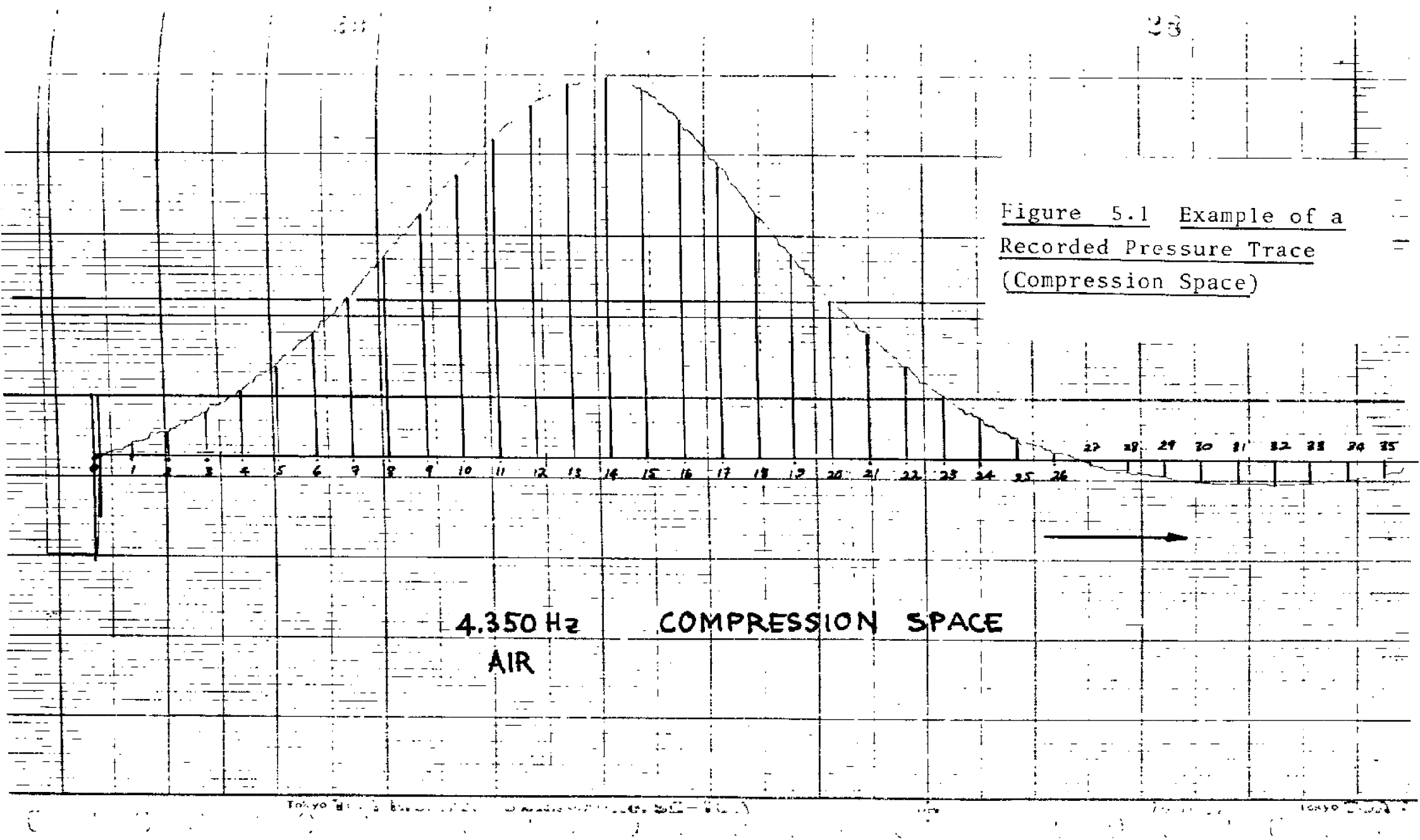

Figure 5.1 Example of a Recorded Pressure Trace (Compression Space)

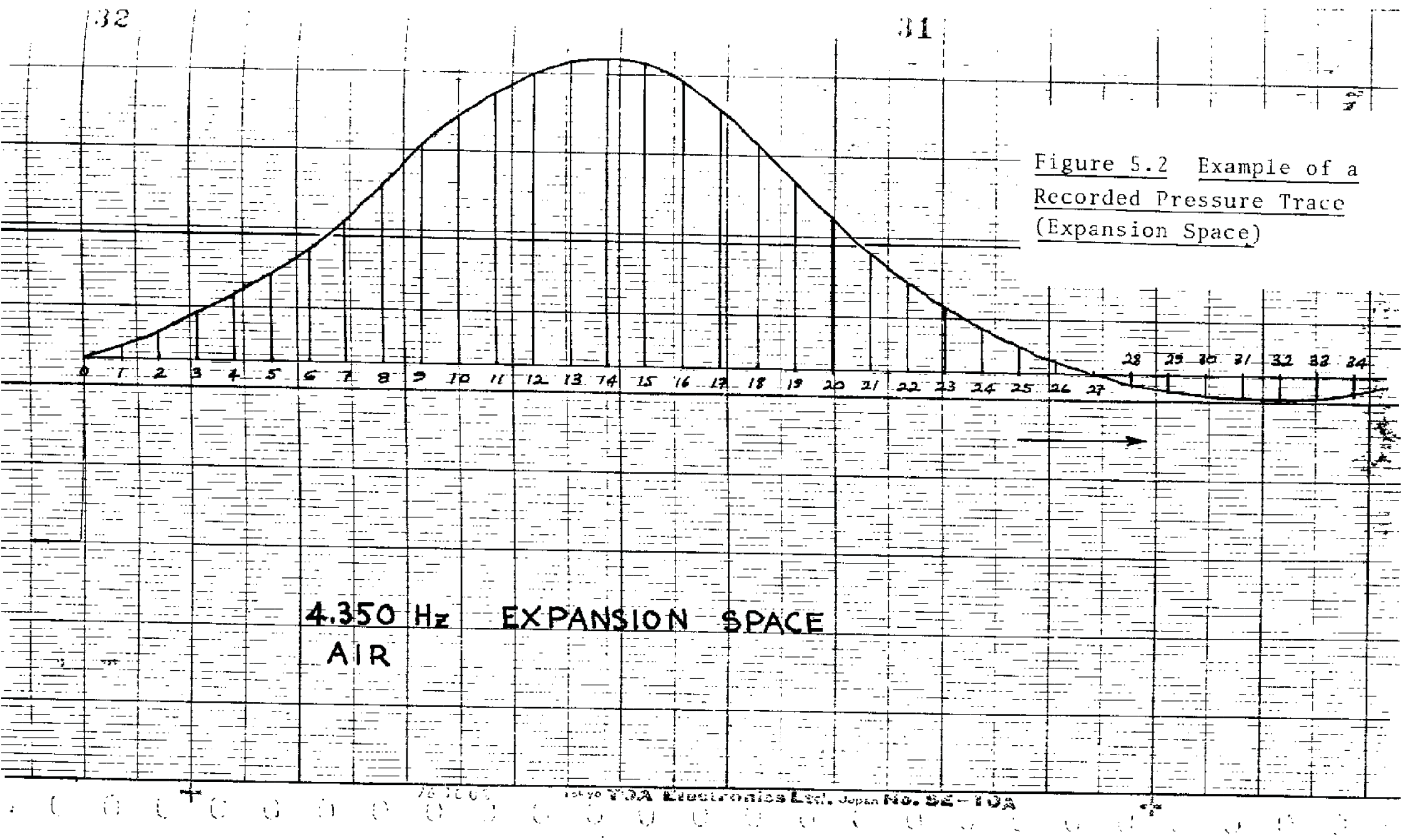

Figure 5.2 Example of a Recorded Pressure Trace (Expansion Space)

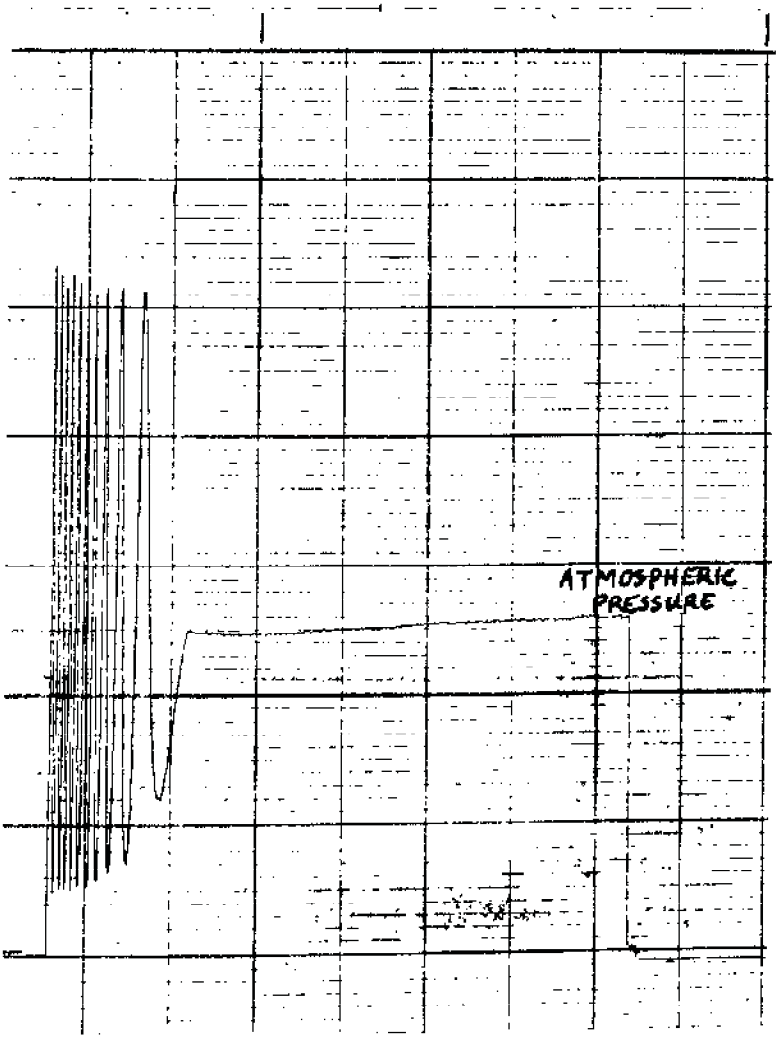

Figure 5.3 Example of a Recorded Decaying Pressure Trace

5.4 Temperature Measurement

The temperature measurement procedure was as follows:

1) The datalogger was programmed according to the manufacturer's instructions. A two minute interval was included between each scan.
2) The datalogger was also used to determine whether the rig had reached thermal equilibrium. Printouts were therefore maintained throughout the experiment.

A sample printout of the temperatures is given in Figure 5.4.

```
25        21,4   t
24        20,4   t
23        94,3   t
22    -   75,2   t
21    -   32,5   t
20        69,5   t
18    -    3,5   t
17        26,4   t
16        33,5   t
15    -   69,4   t
14    -   71,3   t
13    -   67,4   t.
12    -   48,1   t
11    -   11,6   t
10         3,3   t
 9        16,2   t
 8        28,9   t
 7        43,9   t
 6        79,3   t
 5        93,4   t
 4        93,9   t
 3        93,6   t
 2        41,3   t
 1        49,4   t
 0        43,9   t

      000009
013:16:23:16
```

See Appendix Q for thermocouple locations.

Figure 5.4 Temperature Printout

5.5. Energy Balances

The energy balances were determined for both stationary and running conditions. The procedure was as follows (for either condition):

1) When thermal equilibrium had been attained, the condensate was collected over a period of twenty minutes and its mass determined. The volume of CO_2 gas given off was determined over the same period.

2) During this period the temperature gradients, the temperature of the steam and the dry ice mixture, and the temperature at the gas meter were also determined.
3) The ambient conditions of pressure and temperature were measured.
4) Using the results derived in Appendix M, the relevant heat flows were calculated.

A sample calculation is presented in Appendix R.

6 EXPERIMENTAL AND SIMULATION RESULTS

Introduction

Three experimental runs were made at the following speeds: 2,50 Hz, 3,35 Hz and 4,35 Hz which covered the complete speed range of the rig.

The following experimental and simulation comparisons are presented:

1) pressure profiles (Figures 6.1 to 6.9)
2) wall temperature distribution (Figures 6.10 to 6.12)
3) work rate and cyclic work (Figures 6.13 to 6.15)
4) cyclic heat transferred (Figures 6.16 to 6.18)
5) average temperatures in the working spaces (Figures 6.22 to 6.24).

The momentum equation has been evaluated using the 'upstream' technique for all the speeds. The central difference technique has been evaluated for comparison at the highest speed only (Figures 6.25 to 6.32).

Simulation heat rates and working spaces temperature profiles are also presented (Figures 6.16 to 6.24).

Three-dimensional surfaces of the simulation results are included for qualitative purposes only. These results are:

1) pressure versus theta and position in the machine (Figure 6.33)
2) working gas temperature versus theta and position in the machine (Figure 6.34)
3) mass flux density versus theta and position in the machine (Figure 6.35)

All the three-dimensional surfaces are presented for the highest speed only (4,350 Hz).

The graphical symbols plotted on the curves are for tagging purposes only. All the curves are continuous to the size of one differential increment. For the simulated wall temperature distribution, however, each symbol does indicate a discrete calculated point. These points are connected by straight lines.

All simulation runs were done for five cooler cells, eleven regenerator cells and five heater cells. This was found to give good results commensurate with low computational times.

The experimental pressure profiles have been reconstructed for plotting purposes by using a Fourier series [Sp71]. Thirty six sample points were used for the 4,35 Hz and 3,35 Hz runs and eighteen for the 2,50 Hz run. Only the first six harmonics were used since the seventh and higher harmonics were found to be negligible. This procedure introduces a further error into the experimental pressure profiles. From Appendix O, the average highest expected error here is approximately $\pm$ 1%.

The experimental work rate (ie, the pdV/dt term) has also been evaluated using the Fourier series representation of the pressure profiles. The average highest expected error in this profile is $\pm$ 5,3% and in the cyclic work, approximately $\pm$ 5,3%.

Note that the plot error indicated on each graph does not refer to the simulation or experimental results. This is simply the error associated with the plotting process.

Truncation errors in the simulation technique have not been calculated. However, comparing double precision output with single precision output, round-off errors were found to be less than 1%. It is expected that the truncation errors will be larger than this, and will therefore predominate.